BJR

https://doi.org/10.1259/bjr.20190289

Received: 24 March 2019 | Revised: 22 September 2019 | Accepted: 11 October 2019

Cite this article as:
Kar J, Cohen MV, McQuiston SA, Figarola MS, Malozzi CM. Fully automated and comprehensive MRI-based left-ventricular contractility analysis in post-chemotherapy breast cancer patients. *Br J Radiol* 2020; **93**: 20190289.

FULL PAPER

Fully automated and comprehensive MRI-based left-ventricular contractility analysis in post-chemotherapy breast cancer patients

[1]JULIA KAR, PhD, [2]MICHAEL V. COHEN, MD, [3]SAMUEL A. MCQUISTON, MD, [3]MARIA S. FIGAROLA, MD and [2]CHRISTOPHER M. MALOZZI, DO

[1]Departments of Mechanical Engineering and Pharmacology, University of South Alabama, 150 Jaguar Drive, Mobile, AL 36688, United States
[2]Department of Cardiology, College of Medicine University of South Alabama, 1700 Center Street, Mobile, AL 36604, United States
[3]Department of Radiology, University of South Alabama, 2451 USA Medical Center Drive, Mobile, AL 36617, United States

Address correspondence to: Dr Julia Kar
E-mail: *jkar@southalabama.edu*

Objective: This study investigated the occurrence of cardiotoxicity-related left-ventricular (LV) contractile dysfunction in breast cancer patients following treatment with antineoplastic chemotherapy agents.
Methods: A validated and automated MRI-based LV contractility analysis tool consisting of quantization-based boundary detection, unwrapping of image phases and the meshfree Radial Point Interpolation Method was used toward measuring LV chamber quantifications (LVCQ), three-dimensional strains and torsions in patients and healthy subjects. Data were acquired with the Displacement Encoding with Stimulated Echoes (DENSE) sequence on 21 female patients and 21 age-matched healthy females. Estimates of patient LVCQs from DENSE acquisitions were validated in comparison to similar steady-state free precession measurements and their strain results validated via Bland–Altman interobserver agreements. The occurrence of LV abnormalities was investigated via significant differences in contractility measurements (LVCQs, strains and torsions) between patients and healthy subjects.
Results: Repeated measures analysis showed similarities between LVCQ measurements from DENSE and steady-state free precession, including cardiac output (4.7 ± 0.4 L, 4.6 ± 0.4 L, $p = 0.8$), and LV ejection fractions (59±6%, 58±5%, $p = 0.2$). Differences found between patients and healthy subjects included enlarged basal diameter (5.0 ± 0.5 cm *vs* 4.4 ± 0.5 cm, $p < 0.01$), apical torsion (6.0 ± 1.1° *vs* 9.7 ± 1.4°, $p < 0.001$) and global longitudinal strain (−0.15 ± 0.02 vs. -0.21 ± 0.04, $p < 0.001$), but not LV ejection fraction (59±6% vs. 63±6%, $p = 0.1$).
Conclusion: The results from the statistical analysis reveal the possibility of LV abnormalities in the post-chemotherapy patients via enlarged basal diameter and reduced longitudinal strain and torsion, in comparison to healthy subjects.
Advances in knowledge: This study shows that subclinical LV abnormalities in post-chemotherapy breast cancer patients can be detected with an automated technique for the comprehensive analysis of contractile parameters.

INTRODUCTION

Administration of the anthracycline and trastuzumab types of antineoplastic chemotherapy agents (CTA) in breast cancer patients often lead to the development of cardiotoxicity, which may counter the gains in survivorship achieved with treatment.[1–4] The epidemiological extent of left-ventricular (LV) dysfunctions and their recurrence caused by CTA cardiotoxicity range from arrhythmias to irreversible heart failure that ultimately requires managed care and guideline-directed medical therapy (GDMT).[5–7] To reduce the burden of this epidemiology, CTA treatment plans must incorporate routine cardiotoxicity surveillance.[1,7–14] The close monitoring of LV contractility during the surveillance period can target early, subclinical detections of myocardial dysfunction and lead to preventive interventions with drugs like enalapril and carvedilol.[1,6,14,15] However, a decline in echocardiographic quantification of LV ejection fraction (LVEF) is the standard accepted measure of cardiotoxicity, which may not always provide optimal information toward subclinical detection.[2,5,9,13] Furthermore, scientific evidence now shows that subclinical LV contractile abnormalities can be effectively monitored by computations of three-dimensional (3D) myocardial strains, which recently were found to be more sensitive biomarkers than LVEF-related measurements.[9,13,16–22]

Hence, the medical community is now focused on more robust surveillance techniques via imaging modalities that incorporate both LVEF and LV strain analysis toward early, subclinical detections of cardiotoxicity-related dysfunction.[10,13,17,18,21,22] To conduct this surveillance effectively, an ideal contractility analysis tool is required that provides comprehensive details on LV chamber quantifications (LVCQ) and 3D strains while being a time-saving and least interventional procedure.

This study investigated the feasibility of a validated and automated, single-scan, MRI-based methodology for contractility analysis toward detecting any LV structural abnormalities or dysfunction that may have occurred in breast cancer survivors who underwent CTA-based chemotherapy.[23] In the context of contractility analysis, structural abnormalities refer to the significant differences found in LV chamber dimensions and quantities and dysfunction (functional abnormalities) refers to similar differences found in LV strains and torsions, in comparison to healthy subjects. Computations of LVCQs were conducted using the contractility analysis tool created for the above methodology from data acquired via the MRI sequence of Displacement Encoding with Stimulated Echoes (DENSE).[24–27] 3D LV strains were analyzed with the strain analysis component of the tool, following which estimates of both LVCQ and 3D strains were compared to age-matched healthy subjects.

METHODS AND MATERIALS

Scope of the study

As mentioned above, this study investigated CTA treatment-related cardiotoxicity with a validated and automated, single-scan MRI-based contractility analysis tool developed for clinical applications.[24–27] The entire algorithm includes code and user-interface for LVCQ, 3D strain and torsional analysis that is implemented in Matlab (Mathworks Inc., Natick, MA). To conduct the analysis the algorithm's main modules perform unwrapping of phase images and quantization of magnitude images that are obtained with the navigator-gated, spiral, 3D DENSE sequence.[27–32] The patient subpopulation investigated for this study were female post-chemotherapy breast cancer patients who had undergone CTA-based treatment. The main validation for this study was repeated measures ANOVA analysis between LVCQs estimated from DENSE and steady-state free precession (SSFP) acquisitions in patients. This validation was conducted to demonstrate the LVCQ algorithm's consistency in generating results from DENSE that were similar to results from a gold-standard sequence, SSFP. This validation approach in patients is similar to previous studies where it was shown that 3D strains evaluated with DENSE were comparable to evaluations with the gold-standard of tagged-MRI.[25,26] All contractile parameters measured in the patient subpopulation were compared to similar measurements in an equal number of age-matched healthy females.

Human subject recruitments

The possible occurrence of LV structural and functional abnormalities was tested on DENSE data acquired from $N = 21$ adult, post-chemotherapy breast cancer survivors. The patients had undergone CTA-based (anthracyclines and trastuzumab) chemotherapy and were under continued surveillance and some under a regimen of managed care for non-acute cardiac complications related to cardiotoxicity (rated at NYHA class = II or less). To rule out the effects of acute comorbidity influencing the results of LV strains from cardiotoxicity, the exclusion criteria for patients included LVEF less than 50%, valvular heart disease, ischemic heart disease and acute infarction, severe hypertension and a terminal life expectancy of fewer than 3 months. Overall, a preserved, TTE-measured LVEF higher than 50% at the inception of chemotherapy was the most important criteria for recruitment. Due to the likelihood of developing common cardiac side-effects following chemotherapy, patients were not excluded if they had developed non-acute conditions that often follow CTA-based chemotherapy, such as arrhythmias without atrial or ventricular fibrillation and hypertension.[1,33] Hence, patients who had developed post-chemotherapy comorbidities rated above NYHA Class II were not included. Radiation therapy is an integral component of the management of breast cancer that effectively reduces local recurrence and like other studies the patients who underwent radiation therapy were not excluded.[9,14,16] The timeline for recruiting patients was within 12 months from the end of their chemotherapy such that strain analysis was conducted when the most clinically relevant form of cardiotoxicity occurs.[10,14] It is noted that confining recruitment within this timeframe was too early for radiotherapy effects to manifest, where aggregate incidence reports show that cardiac complications due to radiation occur after 5–10 years of treatment.[34] The MRI study in each patient was scheduled within a 3 days window following a post-chemotherapy TTE exam to ensure their DENSE and TTE-based LVEFs were comparable. They were consecutively recruited following their cardiologist's referral, given they met the above cardiac risk criteria and had completed their post-chemotherapy TTE. The CTA treatment each patient underwent was either one of the following regimens with individual patient-based modifications, including 1. 60 mg/m^2 of doxorubicin (anthracycline) for four cycles, cyclophosphamide and taxol or, 2. 8 mg/kg loading +6 mg/kg trastuzumab, taxol, carboplatin with/without pertuzumab. Additional full LV short-axis data with SSFP were acquired in the patients to validate their LVEF measurements. Informed consent was signed by patients and healthy subjects based on Institutional Review Board guidelines and patients volunteered access to their medical histories. DENSE acquisitions in $N = 21$ healthy female subjects contributed to the 1:1 age-matched comparison of contractile parameters, with subjects either newly recruited or their data taken from an existing database.[24–27]

DENSE acquisition and protocols

Navigator-gated, spiral 3D DENSE data were acquired on a 1.5 T MAGNETOM Espree (Siemens Healthcare, Erlangen, Germany) scanner with displacement encoding applied in two orthogonal in-plane directions and one through-plane direction.[26,28,29,32] A flexible, anterior 8-channel body matrix RF coil (Siemens Healthcare, Erlanger, Germany) and the table-mounted spine matrix RF coil were used for receiving signals. Typical imaging parameters included field of view (FOV) of 380 × 380 mm^2, echo time (TE) of 1.04 ms, repetition time (TR) of 15 ms, flip angle (FA) of 20°, matrix size of 128 × 128×19, 2.97 × 2.97×5 mm voxel

Table 1. Demographics, comorbidities and chemotherapy doses in patients and healthy subjects

Parameter	Patients	Age-matched HS	*p*-value
Demographics			
Count (females)	21	21	--
Age (years)	55 ± 8.8	54.5 ± 6.6	0.9
DBP (mmHg)	73.8 ± 11.7	69.5 ± 7.8	0.2
SBP (mmHg)	124.7 ± 14.1	123.8 ± 10.7	0.9
HR (bpm)	73.5 ± 11	71.2 ± 8.3	0.5
Body Mass (kg)	72.5 ± 14.6	72.7 ± 12.9	1.0
BMI (kg/m^2)	27.0 ± 4.5	27.2 ± 4.4	0.9
BSA (m^2)	1.8 ± 0.2	1.8 ± 0.2	1.0
Comorbidities			
Hypertension	5	0	0.02*
Hypercholesterolemia	4	0	0.04*
Diabetes mellitus	5	0	0.02*
Chemotherapy dose			
Doxorubicin 240 mg/m^2	14	-	-
Trastuzumab 8 mg/kg loading + 6 mg/kg/cycle	7	-	-
Radiotherapy	8	-	-

HS, healthy subjects; DBP, diastolic blood pressure; SBP, systolic blood pressure; HR, heart rate; BMI, body mass index; BSA, body surface area.
[a]indicates significant differences between patients and healthy subjects.

size, 21 cardiac phases, encoding frequency of 0.06 cycles/mm, simple 4-point encoding and 3-point phase cycling for artefact suppression.[31,32] The number of navigator-accepted heartbeats to complete a single partition in 3D is 36 heartbeats given that three are needed to acquire a complete set of spirals for a single displacement encoding direction and a single phase cycling point.[32] SSFP acquisition consisted of a FOV of 340 × 276 mm, TE of 1.48 ms, TR of 51.15 ms, FA of 80°, matrix size of 192 × 156 × 12, 1.77 × 1.77 mm pixel size, slice thickness of 7 mm and 25 cardiac phases. Heart rates (HR) and blood pressures (BP) were continuously monitored during the scans.

Table 2. Repeated measures analysis between DENSE and SSFP acquisition-based chamber quantifications in patients (*N* = 21), estimated using the automated algorithm

Parameter	DENSE[a]	SSFP[a]	*p*-value[b]
Chamber quantifications			
Dia basal (D) (cm)	5.0 ± 0.5	4.9 ± 0.5	0.9
Dia basal (S) (cm)	3.3 ± 0.4	3.2 ± 0.3	0.8
LV EDV (cm^3)	108 ± 17	107 ± 19	1.0
LV ESV (cm^3)	44 ± 8	45 ± 9	0.8
LV SV (cm^3)	64 ± 14	62 ± 15	0.8
LV EF (%)	59 ± 6	58 ± 5	0.2
CO (L/min)	4.7 ± 0.4	4.6 ± 0.4	0.8
LVM (gm)	123 ± 9	121 ± 12	0.4

CO, cardiac output; D, diastolic;Dia, diameter; EDV, end diastolic volume; EF, ejection fraction; ESV, end systolic volume; LVM, LV mass; S: systolic, SV: stroke volume.
[a]Estimated with the new automated algorithm in *N* = 21 patients.
[b]From repeated measures analysis.

Automated boundary detection

As outlined in our previous study, this automated process consists of first identifying the LV boundary contours in the most basal short-axis slice at end-diastole with the operator selecting an ellipsoidal region of interest (ROI). The above is followed by propagating the boundaries to all end-diastolic short-axis slice positions from base to apex, after which boundary detection occurs incrementally until reaching end-systole.[27] The LV boundaries and intramural tissue are identified using Otsu's Method which is a non-uniform quantization scheme based on image histogram bins that yields a threshold-based image with a distinct profile of the short-axis.[35,36] Otsu's algorithm can separate two or more classes of pixels based on a bimodal (multimodal) histogram distribution once it calculates the optimum thresholds for maximizing interclass variances.[35,36] The strategy for detecting the location of each boundary point consists of computing image gradients based on the quantized pixel intensities. Points on the initial bounding ellipse can then be moved radially across the LV myocardium to detect peaks via the abrupt changes in intensities. To accurately relocate a boundary point at each timeframe the positioning based on the quantized profile was additionally guided by DENSE phase-based displacements at pixels nearest to that point.[25,28,29,32,37] The raw displacement data were refined using temporal fitting of each pixel's trajectory with a fifth-order Fourier basis functions.[25,26,29,32] Following the

Table 3. Comparisons of chamber quantifications and strains estimated with the automated algorithm between patients and healthy subjects

Parameter	Patients	Age-matched HS	*p*-value
Count (females)	21	21	--
Chamber quantifications			
Dia basal (D) (cm)	5.0 ± 0.5	4.4 ± 0.5	0.0*
Dia basal (S) (cm)	3.3 ± 0.4	2.7 ± 0.4	0.0*
LV EDV (cm^3)	108 ± 17	111 ± 18	0.7
LV ESV (cm^3)	44 ± 8	42 ± 11	0.5
LV SV (cm^3)	64 ± 14	69 ± 13	0.3
LV EF (%)	59 ± 6	63 ± 6	0.1
LVM (gm)	123 ± 9	126 ± 10	0.1
LVM/BSA (gm/m^2)	68 ± 8	71 ± 9	0.4
Strains and torsion			
E_{cc} Basal	−0.18 ± 0.03	−0.20 ± 0.02	0.2
E_{cc} Mid	−0.20 ± 0.03	−0.21 ± 0.03	0.3
E_{cc} Apical	−0.22 ± 0.03	−0.24 ± 0.04	0.2
E_{cc} Global	−0.20 ± 0.03	−0.21 ± 0.03	0.2
E_{ll} Basal	−0.14 ± 0.02	−0.19 ± 0.05	0.0**
E_{ll} Mid	−0.15 ± 0.02	−0.21 ± 0.04	0.0**
E_{ll} Apical	−0.16 ± 0.03	−0.23 ± 0.04	0.0**
E_{ll} Global	−0.15 ± 0.02	−0.21 ± 0.04	0.0**
E_{rr} Basal	0.38 ± 0.05	0.38 ± 0.05	0.9
E_{rr} Mid	0.32 ± 0.04	0.34 ± 0.04	0.2
E_{rr} Apical	0.26 ± 0.04	0.27 ± 0.03	0.1
E_{rr} Global	0.32 ± 0.04	0.33 ± 0.04	0.4
Rotation basal (^{O})	−1.50 ± 1.10	−4.50 ± 2.10	0.0**
Rotation mid (^{O})	5.50 ± 1.50	8.30 ± 1.90	0.0**
Rotation apex (^{O})	8.30 ± 2.10	11.70 ± 2.50	0.0**
Torsion basal (^{O})	0.00 ± 0.00	0.00 ± 0.00	-
Torsion mid (^{O})	4.80 ± 0.98	7.70 ± 1.30	0.0**
Torsion apical (^{O})	6.00 ± 1.10	9.70 ± 1.40	0.0**

Dia, diameter; HS, healthy subjects; D, diastolic; S, systolic; EDV, end diastolic volume; ESV, end systolic volume; SV, stroke volume; EF, ejection fraction; LVM, LV mass; BSA, body surface area; rr, radial; cc; circumferential.
[a]Indicates significant differences between patients and healthy subjects at $p < 0.01$.
[b]Indicates significant differences at $p < 0.001$.

generation of boundaries and 3D LV reconstruction, LVCQs estimated from DENSE and SSFP images included measuring the end-diastolic diameter (EDD), end-systolic diameter (ESD), end-diastolic volume (EDV), end-systolic volume (ESV), stroke volume (SV), LVEF and LV mass (LVM).[27]

Meshfree strain analysis

3D strain tensors were computed using the radial point interpolation method (RPIM) at each voxel in the patient's reconstructed 3D geometries. RPIM is a numerical analysis technique based on the Galerkin weak form, details on which methodology for computing 3D LV strains, via incorporating Multiquadrics (MQ) shape functions for radial basis function (RBF) evaluations, are given in previous literature.[25,26,38–40] The raw displacement data for computing 3D strains were from the unwrapping of phase images acquired with the DENSE sequence. Another important target was to determine LV torsion that characteristically defines the contraction–relaxation behavior of the spiraling myofibers. The definition of LV torsion used was the relative angle of twist between basal and apical rotations multiplied by the ratio of the mean segmental radius to the intersegment distance, given by,[41]

$$\alpha_T = \frac{(\varphi_{base} - \varphi_{apex})(\rho_{base} + \rho_{apex})}{2D} \quad (1)$$

Figure 1. (a) The superposition of stacks of DENSE (green rim) and SSFP (red rim) LV short-axis frames that were acquired at similar planar orientations for comparing chamber quantifications. (b) Bland–Altman agreement between LVEF estimated from DENSE and SSFP acquisitions with the automated contractility analysis tool in N = 21 patients. (c) Diastolic and systolic short-axis slices acquired with DENSE and SSFP from a similar mid-ventricular orientation. DENSE, DisplacementEncoding with Stimulated Echoes; SSFP, steady-state free precession.

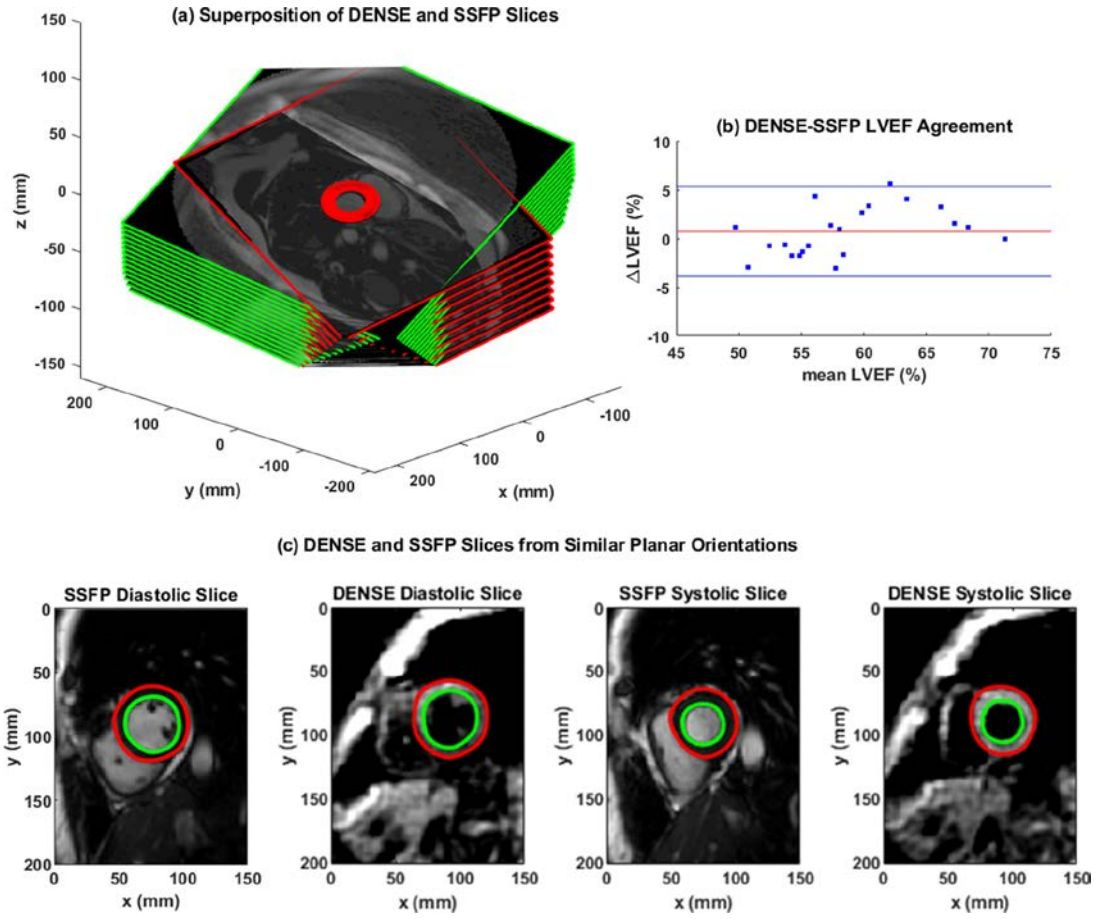

where φ is the angle of twist, ρ is the radius, and D is the inter segment distance. It is a definition of torsion that requires only the displacement vectors and computations of myocardial boundaries or Lagrangian strains are not necessary.

Statistical analysis

Means and standard deviations were computed for demographic data, LVCQs, strains and torsions. To validate the LVCQ analysis, repeated measures analysis was conducted between patient LVCQs estimated with it from DENSE and SSFP same-day acquisitions. Additionally, repeated measures analysis was conducted between the DENSE, SSFP and TTE exam-based LVEF measurements in patients following chemotherapy. All repeated measures ANOVA were estimated with SPSS, v. 26 (IBM Corp., Armonk, NY) which included a Mauchly's test for sphericity and any significant differences from the results of within-subjects effects reported. Agreements were assessed between the DENSE- and SSFP-based regional epicardial and endocardial bounded areas to estimate geometric variances arising from the displacement-guided boundary searches. Bland–Altman interobserver agreements were assessed for patient strains measured within the detected boundaries, with random segmentation and strain analysis conducted by two independent users (a radiology researcher and a graduate engineer). Comparisons of contractile parameters between patients and age-matched healthy subjects were conducted with unpaired two-sample t-tests and significant differences due to LV structural abnormalities and dysfunction observed.[42,43]

RESULTS

The demographic information on age-matched patients and healthy subjects are given in Table 1, which also details existing comorbidities in patients and their chemotherapy treatment plans. The MRI scans were scheduled within 3 days of a routine post-chemotherapy TTE to ensure accuracy of comparisons between DENSE, SSFP and TTE LVEF results. The time to recruiting patients from the end of chemotherapy was 5.7 ± 3.8 months. Table 2 shows the results of repeated measures analysis between LVCQs estimated from DENSE and SSFP acquisitions in patients with significant differences not found between these measurements, which was an important finding related to the newly validated automated segmentation technique.[27] The Fisher statistics from repeated measures analysis between results of patient LVEFs from DENSE (59±6%), SSFP (58±5%)

Figure 2. The 3D displacement vectors computed from phase-unwrapping and fitted with fifth-order Fourier basis function in the full LV of (a) a patient and (b) a healthy subject. 3D,three-dimensional; LV, left-ventricular.

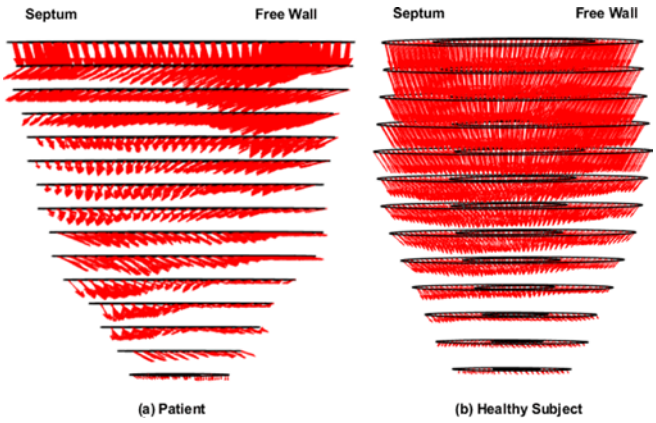

and post-chemotherapy TTE (58±7%) was $F(2, 40)=1.8$, $p = 0.2$ without sphericity assumption violated, showing that a significant difference was not there between the measurements. Estimates of contractile parameters consisting of LVCQs, strains and torsions in patients and healthy subjects are given in Table 3.

Figure 1(a) shows overlapped stacks of DENSE and SSFP short-axis slices such that LVCQ comparisons, including areas, cavity volumes and LVEF, were conducted within similarly located boundaries from the two protocols. Figure 1(b) shows the agreement between LVEFs estimated in patients with the two protocols. The similarities in short-axis profiles and myocardial boundaries detected from nearly overlapped slices are shown in Figure 1(c). Agreements between the regional systolic areas obtained with the two protocols for the epicardium and endocardium are given in Supplementary Material 1, which did not differ significantly in a similar way to their diameters (Table 2). Figure 2 shows the trend in DENSE-based 3D displacement differences that emerged between patients and healthy subjects. The interobserver agreements on the normal strains and torsions in patients, with the newly validated segmentation approach integrated into the contractility analysis tool, are shown in Figure 3(a)–(d).[21] This agreement found with several hundred systolic frames followed the displacement-guided segmentation process that was conducted in approximately 11,500 DENSE short-axis slices (patients and healthy subjects combined), comprising of spatiotemporal frames and apex to base for the duration of systole. With the above total number of frames processed, the automated algorithm failed in approximately 400 frames amounting to a segmentation success rate of ~97%. The processing time per segmentation was less than 2 s with a 3.4 GHz Intel Core processor and 16 GB RAM in a 64-bit operating system and therefore approximately 8.5 min were required for analyzing each LV. The majority of this computational expense involved time spent in phase-unwrapping, conducting the Fourier fitting and image rendering tasks. Figure 4 shows trajectories of fitted contractile parameters including the three normal strains, LVEF and apical torsion in both patients and healthy subjects. Temporal fitting for trajectories in Figure 4 was with

Figure 3. Interobserver agreements established with Bland–Altman analysis for basal, mid-ventricular and apical radial, circumferential and longitudinal strains and mid-ventricular and apical torsions in the LV, computed with the 3D automated strain analysis algorithm in $N = 21$ patients. 3D,three-dimensional; LV, left-ventricular.

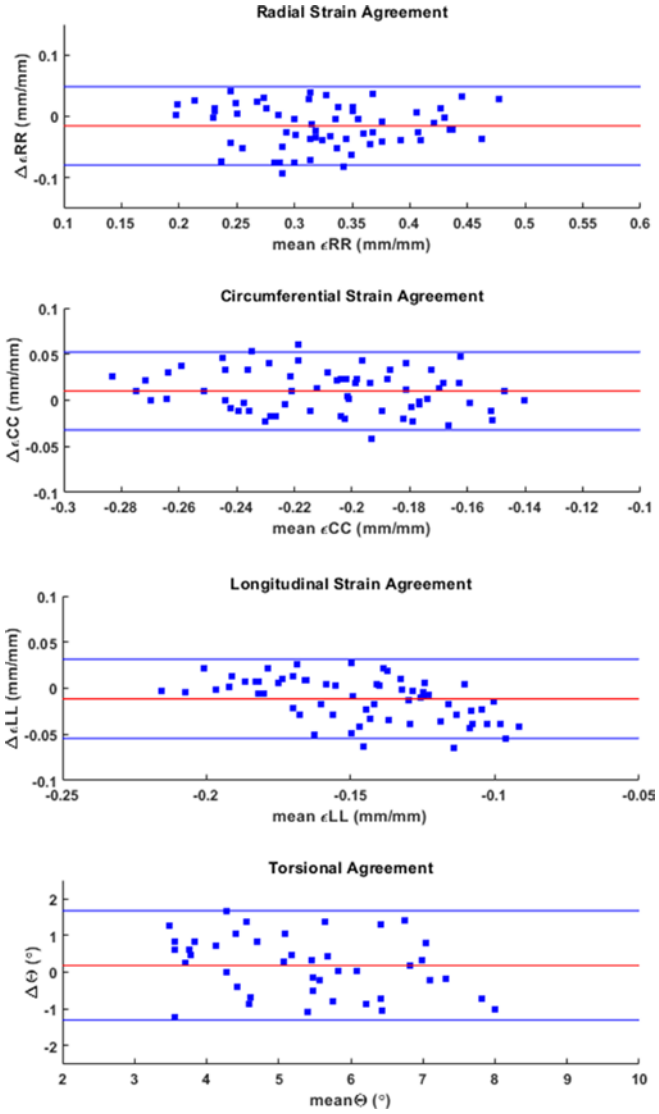

fifth-order Fourier basis functions in the same way as displacement vectors were fitted. Data were extrapolated beyond the number of cardiac phases acquired to show at least one period for each contractile parameter. It is seen from Figure 4 that the peak longitudinal strain and torsion in patients are significantly different from healthy subjects, but not peak LVEF and radial and circumferential strains, as also given in Table 3. Furthermore, Table 3 shows the significantly different rotations between groups with it being a fundamental parameter for computing torsion. Figure 5 shows 3D surface maps of the full LV for circumferential and longitudinal strains and torsion in a patient and healthy subject at systole. The patient LV basal diameter is slightly enlarged which is representative of the patient subpopulation. Furthermore, Figure 5 shows reduced longitudinal strain and torsion in the patient when compared to the healthy subject

Figure 4. Systolic trajectories of global circumferential, longitudinal and radial strains (mm/mm), apical torsion (°) and LVEF (%) estimated in the patient subpopulation (*N* = 21) and healthy subjects (*N* = 21). LVEF, LV ejection fraction.

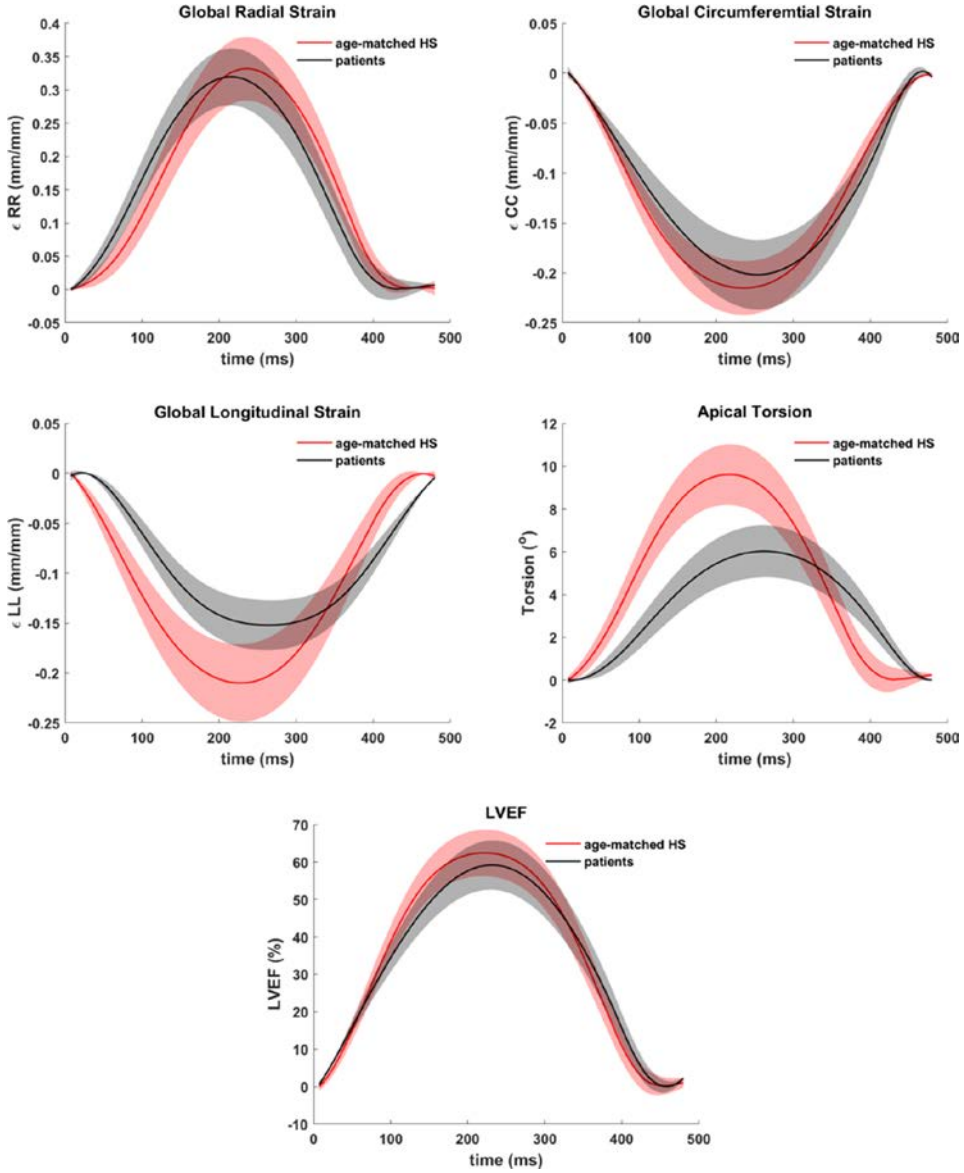

but the circumferential strain ranges are closer between the two representatives.

Discussion

This study applied a validated and automated methodology for determining LV contractile parameters in a subpopulation of breast cancer patients (with profiles given in Table 1) who have enhanced risks of developing cardiotoxicity. Systolic contractile parameters of the LV were computed with displacement-guided motion tracking for LVCQs and meshfree RPIM strain analysis, which are both validated components of this tool.[24–27] Given in Table 2 are the results of LVCQ analysis and validation in the patient subpopulation with between-protocols repeated measures analysis, which is also visually represented in Figure 1 via the similarities in acquisitions. This was indeed an important outcome that showed the DENSE-based results validated in comparison to the gold-standard protocol of SSFP. Also noted is that these similarities were achieved with several thousand short-axis slices successfully undergoing the contractility analysis steps. It was proven yet again by the Fisher statistical result from the next repeated measures analysis showing that a significant difference between DENSE, SSFP and TTE-based LVEFs did not exist. However, while automating segmentations in ~97% of the images indicates a high success rate, there is potential for failure under certain circumstances. Such failed attempts generally occurred due to a lack of contrast (or quality) in the magnitude images in the timeframes following the systolic phase or similarly from unwrapping errors. Differences in segmented areas between SSFP and DENSE were non-significant, for both epicardium and endocardium, and the low biases and narrow limits from assessing their agreements are shown in Supplementary Material 1. Similar to the repeated measures analyses, it is yet another validation of the DENSE displacement-guided LVCQ results. It also shows that an LVCQ tool that saves valuable time

Figure 5. Three-dimensional circumferential and longitudinal strain and torsional surface maps generated with the automated strain analysis algorithm in the full LV of (a) a patient and (b) a healthy subject. A, anterior; AS, anteroseptal; PS, posteroseptal; P, posterior; PL, posterolateral; AL, anterolateral; LV, left-ventricular.

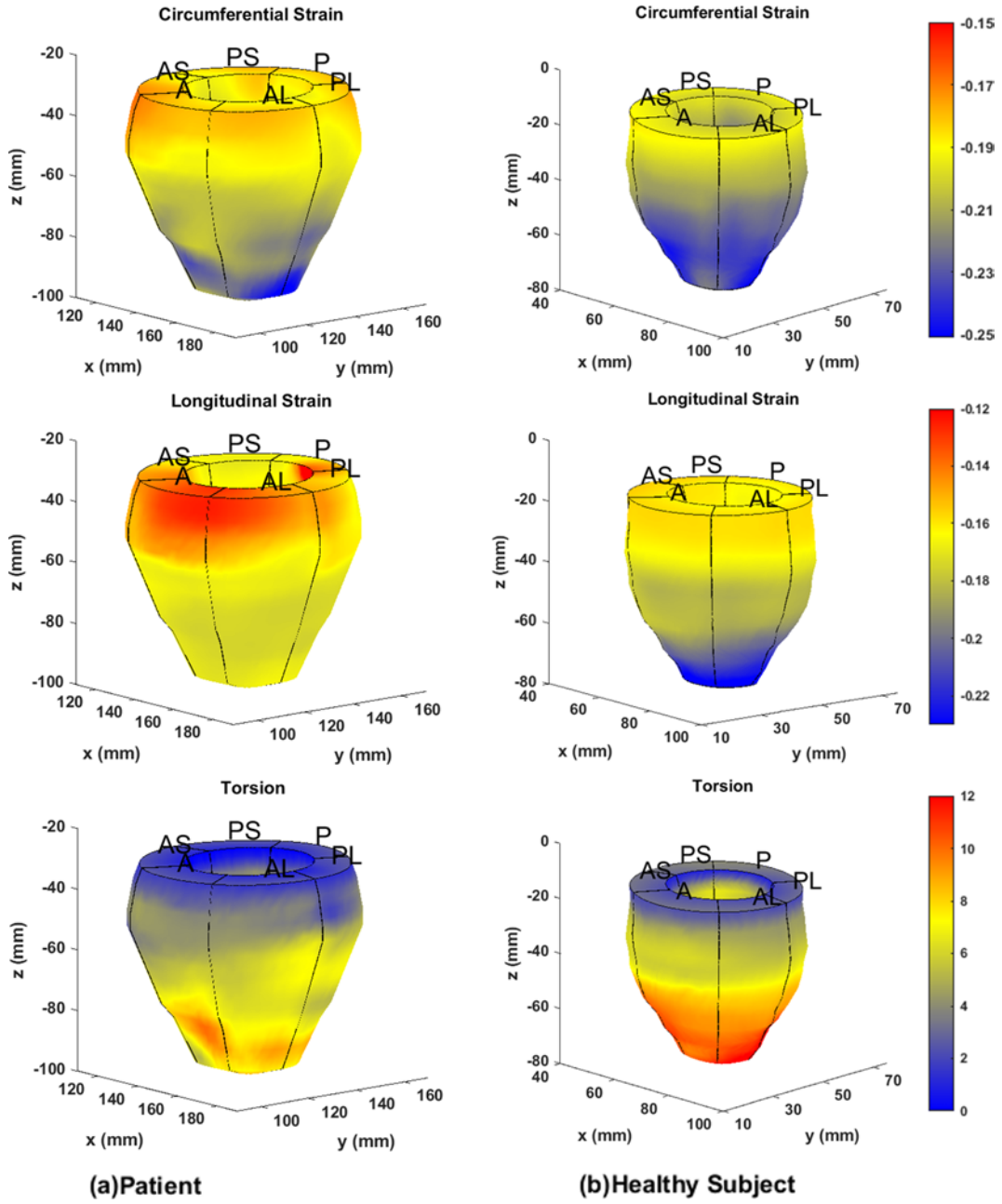

and manual effort can be designed with accurate quantization levels, phase-unwrapping and smoothing techniques. Figure 2 is a visual indicator of LV dysfunction in the patient subpopulation where the disarrangement of displacement vectors show the dyssynchrony in wall-motion and septal dilation that is characteristic to non-ischemic cardiomyopathy.[44] This morphology into cardiomyopathic abnormalities commonly occurs in CTA-induced cardiotoxicity as also reported in numerous previous studies.[1,11,14,15,44,45] Figure 3(a)–(d) show the low biases found with interobserver agreements on the contractile parameters estimated in patients, where the limits did not surpass ~0.06 in strain magnitude and remained less than 1.5° in torsional agreement. The extent of these agreements indicates the soundness of the strain analysis approach and supports the findings of subclinical myocardial abnormalities detected via some of these parameters. Determining these LV contractile parameters that significantly differed between CTA treated patients and age-matched healthy subjects was an important goal of this study, which was found to be in longitudinal strain, torsion and the basal diameter distortion as detailed in Table 3 and visually seen in Figures 4-5. The above key findings are inclusive of not finding significant differences in LVEF and circumferential and radial strain measurements between patients and healthy subjects.

Background research on the consistencies of results between this study and previous ones were conducted.[11,16,46] Primarily, the similarities found with other studies were the LV structural and functional abnormalities that occur when CTA doses of anthracyclines and trastuzumab are administered either separately or in combination.[16,46] Additionally found were similarities to studies that show myocardial dysfunction related to subclinical cardiotoxicity can be detected with altered global and regional strains, either independently or earlier to significant reductions in LVEF.[2,11,13,16,18,47] Analogous results found in these studies include reductions in peak systolic strains with longitudinal strain dropping by 15–20% and torsional reductions of 50% without seeing any LVEF reductions (Figures 4 and 5, Table 3).[9,11,47] This study also showed that strain-based analysis can detect impaired LV functionality within a short period following chemotherapy, like the studies by Sawaya et al, Motoki et al and others.[10,11,13,16,17] The enlargement in basal diameter with preserved LVEF has been seen in previous studies such as the recent Carvedilol for Prevention of Chemotherapy-Related Cardiotoxicity (CECCY) trial which randomized 200 patients with breast cancer tumors receiving anthracyclines and who received a placebo or carvedilol until chemotherapy completion.[15] The explanation for this enlargement lies in cardiomyopathy developing in some patients, which generally arise within a few weeks of concluding chemotherapy and may last several months as reported by the CECCY trial and other studies.[1,14,15] Similarities not found with existing studies include not finding a reduction in peak systolic radial strain which studies have reported dropping by ~25% or in peak systolic circumferential strain dropping by ~15%.[9–12,16,17] In summary, the results of this study were similar to results from several previous studies that investigated cardiotoxicity-related contractile parameters in post-chemotherapy breast cancer patients.

The first limitation is that this study is not a longitudinal study where the appearance and extent of LV abnormalities in the patients were tracked with time. While the pathophysiology related to the development of cardiotoxicity cannot be provided, evidence related to the abnormalities in LV structure and function that developed in patients was found in comparison to ground-truth references in age-matched healthy subjects. The second limitation was that the influence of existing comorbidities (or other cardiac complications) on strain results cannot be quantified and isolated from the contractility analysis on cardiotoxicity. The compounding effects of LV abnormalities due to hypertension, diabetes and others (Table 1) have been reported as non-separable with biomarker analysis in previous studies and currently, a statistical model for separately considering each comorbidity does not exist.[1,10,14,16,46,48] However, the recruitment criteria for this study were designed for the least impact of comorbidities on strain parameters by ensuring that patients had pre-chemotherapy LVEF higher than 50% and comorbidities rated NYHA Class II or less. The third limitation was not investigating the effect of manually contouring the LV boundaries, which can be an extremely tedious process for the full LV. While the possibility exists for improved accuracy with a human perspective on contouring, the prospect of individually contouring more than 10,000 image frames by hand was beyond practical consideration for this study.

CONCLUSION

This study showed the potential of a validated, myocardial displacement-guided contractility analysis tool based on DENSE acquisitions toward investigating cardiac abnormalities that arise from CTA treatment in post-chemotherapy breast cancer patients. The study findings show LV structural abnormalities (enlarged basal diameter) and dysfunction (reduced longitudinal strain and torsion) in the patient subpopulation with completion of treatment, in comparison to similar measurements conducted in age-matched healthy subjects. A final note on the findings is that cardiac complications unrelated to cardiotoxicity or from the existing comorbidities may have influenced the results of strain analysis.

ACKNOWLEDGMENT

We are very appreciative of staff at the Imaging Center, Children's and Women's Hospital, University of South Alabama toward helping us acquire the MRI data. We thank Dr Clive Woods for his help with proof reading and statistical analysis for this study. We greatly appreciate Dr Fredrick Epstein's insight toward acquiring functional DENSE data in this specific patient subpopulation.This project was partially funded by NIH grant 1R21EB028063-01

REFERENCES

1. Cardinale D, Colombo A, Lamantia G, Colombo N, Civelli M, De Giacomi G, et al. Anthracycline-Induced cardiomyopathy: clinical relevance and response to pharmacologic therapy. *J Am Coll Cardiol* 2010; **55**: 213–20. doi: https://doi.org/10.1016/j.jacc.2009.03.095
2. Jurcut R, Wildiers H, Ganame J, D'hooge J, Paridaens R, Voigt J-U. Detection and monitoring of cardiotoxicity-what does modern cardiology offer? *Support Care Cancer* 2008; **16**: 437–45. doi: https://doi.org/10.1007/s00520-007-0397-6
3. Stoodley P, Tanous D, Richards D, Meikle S, Clarke J, Hui R, et al. Trastuzumab-induced cardiotoxicity: the role of two-dimensional myocardial strain imaging in diagnosis and management. *Echocardiography* 2012; **29**: E137–40. doi: https://doi.org/10.1111/j.1540-8175.2011.01645.x
4. Jordan JH, Vasu S, Morgan TM, D'Agostino RB, Meléndez GC, Hamilton CA, et al. Anthracycline-Associated T1 mapping characteristics are elevated independent of the presence of cardiovascular comorbidities in cancer survivors. *Circ Cardiovasc Imaging* 2016; **9**. doi: https://doi.org/10.1161/CIRCIMAGING.115.004325
5. Hunt SA, Abraham WT, Chin MH, Feldman AM, Francis GS, Ganiats TG, et al. ACC/AHA 2005 guideline update for the diagnosis and management of chronic heart failure in the adult: a report of the American College of Cardiology/American heart association Task force on practice

guidelines (writing Committee to update the 2001 guidelines for the evaluation and management of heart failure): developed in collaboration with the American College of chest physicians and the International Society for heart and lung transplantation: endorsed by the heart rhythm Society. *Circulation* 2005; **112**: e154–235. doi: https://doi.org/10.1161/CIRCULATIONAHA.105.167586

6. Curigliano G, Cardinale D, Dent S, Criscitiello C, Aseyev O, Lenihan D, et al. Cardiotoxicity of anticancer treatments: epidemiology, detection, and management. *CA Cancer J Clin* 2016; **66**: 309–25. doi: https://doi.org/10.3322/caac.21341
7. Volkova M, Russell R. 3Rd. anthracycline cardiotoxicity: prevalence, pathogenesis and treatment. *Curr Cardiol Rev* 2012; **7**: 214–20. doi: https://doi.org/10.2174/157340311799960645
8. Slamon D, Eiermann W, Robert N, Pienkowski T, Martin M, Press M, et al. Adjuvant trastuzumab in HER2-positive breast cancer. *N Engl J Med* 2011; **365**: 1273–83. doi: https://doi.org/10.1056/NEJMoa0910383
9. Thavendiranathan P, Poulin F, Lim K-D, Plana JC, Woo A, Marwick TH. Use of myocardial strain imaging by echocardiography for the early detection of cardiotoxicity in patients during and after cancer chemotherapy: a systematic review. *J Am Coll Cardiol* 2014; **63**(25 Pt A): 2751–68. doi: https://doi.org/10.1016/j.jacc.2014.01.073
10. Sawaya H, Sebag IA, Plana JC, Januzzi JL, Ky B, Cohen V, et al. Early detection and prediction of cardiotoxicity in chemotherapy-treated patients. *Am J Cardiol* 2011; **107**: 1375–80. doi: https://doi.org/10.1016/j.amjcard.2011.01.006
11. Motoki H, Koyama J, Nakazawa H, Aizawa K, Kasai H, Izawa A, et al. Torsion analysis in the early detection of anthracycline-mediated cardiomyopathy. *Eur Heart J Cardiovasc Imaging* 2012; **13**: 95–103. doi: https://doi.org/10.1093/ejechocard/jer172
12. Mornoș C, Petrescu L. Early detection of anthracycline-mediated cardiotoxicity: the value of considering both global longitudinal left ventricular strain and twist. *Can J Physiol Pharmacol* 2013; **91**: 601–7. doi: https://doi.org/10.1139/cjpp-2012-0398
13. Jurcut R, Wildiers H, Ganame J, D'hooge J, De Backer J, Denys H, et al. Strain rate imaging detects early cardiac effects of pegylated liposomal doxorubicin as adjuvant therapy in elderly patients with breast cancer. *J Am Soc Echocardiogr* 2008; **21**: 1283–9. doi: https://doi.org/10.1016/j.echo.2008.10.005
14. Cardinale D, Colombo A, Bacchiani G, Tedeschi I, Meroni CA, Veglia F, et al. Early detection of anthracycline cardiotoxicity and improvement with heart failure therapy. *Circulation* 2015; **131**: 1981–8. doi: https://doi.org/10.1161/CIRCULATIONAHA.114.013777
15. Avila MS, Ayub-Ferreira SM, de Barros Wanderley MR, das Dores Cruz F, Gonçalves Brandão SM, Rigaud VOC, et al. Carvedilol for prevention of chemotherapy-related cardiotoxicity: the CECCY trial. *J Am Coll Cardiol* 2018; **71**: 2281–90. doi: https://doi.org/10.1016/j.jacc.2018.02.049
16. Sawaya H, Sebag IA, Plana JC, Januzzi JL, Ky B, Tan TC, et al. Assessment of echocardiography and biomarkers for the extended prediction of cardiotoxicity in patients treated with anthracyclines, taxanes, and trastuzumab. *Circulation* 2012; **5**: 596–603. doi: https://doi.org/10.1161/CIRCIMAGING.112.973321
17. Stoodley PW, Richards DAB, Hui R, Boyd A, Harnett PR, Meikle SR, et al. Two-Dimensional myocardial strain imaging detects changes in left ventricular systolic function immediately after anthracycline chemotherapy. *Eur J Echocardiogr* 2011; **12**: 945–52. doi: https://doi.org/10.1093/ejechocard/jer187
18. Poterucha JT, Kutty S, Lindquist RK, Li L, Eidem BW. Changes in left ventricular longitudinal strain with anthracycline chemotherapy in adolescents precede subsequent decreased left ventricular ejection fraction. *J Am Soc Echocardiogr* 2012; **25**: 733–40. doi: https://doi.org/10.1016/j.echo.2012.04.007
19. Nakano S, Takahashi M, Kimura F, Senoo T, Saeki T, Ueda S, et al. Cardiac magnetic resonance imaging-based myocardial strain study for evaluation of cardiotoxicity in breast cancer patients treated with trastuzumab: a pilot study to evaluate the feasibility of the method. *Cardiol J* 2016; **23**: 270–80. doi: https://doi.org/10.5603/CJ.a2016.0023
20. Grover S, Leong DP, Chakrabarty A, Joerg L, Kotasek D, Cheong K, et al. Left and right ventricular effects of anthracycline and trastuzumab chemotherapy: a prospective study using novel cardiac imaging and biochemical markers. *Int J Cardiol* 2013; **168**: 5465–7. doi: https://doi.org/10.1016/j.ijcard.2013.07.246
21. Mordi I, Bezerra H, Carrick D, Tzemos N. The combined incremental prognostic value of LVEF, late gadolinium enhancement, and global circumferential strain assessed by CMR. *JACC Cardiovasc Imaging* 2015; **8**: 540–9. doi: https://doi.org/10.1016/j.jcmg.2015.02.005
22. Jeung M-Y, Germain P, Croisille P, El ghannudi S, Roy C, Gangi A. Myocardial tagging with MR imaging: overview of normal and pathologic findings. *Radiographics* 2012; **32**: 1381–98. doi: https://doi.org/10.1148/rg.325115098
23. Kar JC, B.P.; Pasque MK. inventor Washington University, assignee. In: *Systems and methods for measuring cardiac strain*: United States patent US20180116521A1; 2018.
24. Kar J, Cupps B, Zhong X, Koerner D, Kulshrestha K, Neudecker S, et al. Preliminary investigation of multiparametric strain Z-score (MPZS) computation using displacement encoding with simulated echoes (dense) and radial point interpretation method (RPIM. *J Magn Reson Imaging* 2016; **44**: 993–1002. doi: https://doi.org/10.1002/jmri.25239
25. Kar J, Knutsen AK, Cupps BP, Pasque MK. A validation of two-dimensional in vivo regional strain computed from displacement encoding with stimulated echoes (dense), in reference to tagged magnetic resonance imaging and studies in repeatability. *Ann Biomed Eng* 2014; **42**: 541–54. doi: https://doi.org/10.1007/s10439-013-0931-2
26. Kar J, Knutsen AK, Cupps BP, Zhong X, Pasque MK. Three-Dimensional regional strain computation method with displacement encoding with stimulated echoes (dense) in non-ischemic, non-valvular dilated cardiomyopathy patients and healthy subjects validated by tagged MRI. *J Magn Reson Imaging* 2015; **41**: 386–96. doi: https://doi.org/10.1002/jmri.24576
27. Kar J, Zhong X, Cohen MV, Cornejo DA, Yates-Judice A, Rel E, et al. Introduction to a mechanism for automated myocardium boundary detection with displacement encoding with stimulated echoes (dense. *Br J Radiol* 2018; **20170841**.
28. Kim D, Gilson WD, Kramer CM, Epstein FH. Myocardial tissue tracking with two-dimensional cine displacement-encoded MR imaging: development and initial evaluation. *Radiology* 2004; **230**: 862–71. doi: https://doi.org/10.1148/radiol.2303021213
29. Spottiswoode BS, Zhong X, Hess AT, Kramer CM, Meintjes EM, Mayosi BM, et al. Tracking myocardial motion from cine dense images using spatiotemporal phase unwrapping and temporal fitting. *IEEE Trans Med Imaging* 2007; **26**: 15–30. doi: https://doi.org/10.1109/TMI.2006.884215
30. Aletras AH, Ding S, Balaban RS, Wen H. Dense: displacement encoding with stimulated echoes in cardiac functional MRI.

J Magn Reson 1999; **137**: 247–52. doi: https://doi.org/10.1006/jmre.1998.1676
31. Zhong X, Gibberman LB, Spottiswoode BS, Gilliam AD, Meyer CH, French BA, et al. Comprehensive cardiovascular magnetic resonance of myocardial mechanics in mice using three-dimensional cine dense. *J Cardiovasc Magn Reson* 2011; **13**: 83. doi: https://doi.org/10.1186/1532-429X-13-83
32. Zhong X, Spottiswoode BS, Meyer CH, Kramer CM, Epstein FH. Imaging three-dimensional myocardial mechanics using navigator-gated volumetric spiral cine dense MRI. *Magn Reson Med* 2010; **64**: 1089–97. doi: https://doi.org/10.1002/mrm.22503
33. McGowan JV, Chung R, Maulik A, Piotrowska I, Walker JM, Yellon DM. Anthracycline chemotherapy and cardiotoxicity. *Cardiovasc Drugs Ther* 2017; **31**: 63–75. doi: https://doi.org/10.1007/s10557-016-6711-0
34. Carver JR, Shapiro CL, Ng A, Jacobs L, Schwartz C, Virgo KS, et al. American Society of clinical oncology clinical evidence review on the ongoing care of adult cancer survivors: cardiac and pulmonary late effects. *JCO* 2007; **25**: 3991–4008. doi: https://doi.org/10.1200/JCO.2007.10.9777
35. Liao PS S. Ct, Chung PC. A fast algorithm for multilevel Thresholding. *J Inf Sci Eng* 2001; **17**: 713–27.
36. Otsu N. A threshold selection method from Gray-Level histograms. *IEEE Trans Syst Man Cybern* 1979; **9**: 62–6. doi: https://doi.org/10.1109/TSMC.1979.4310076
37. Spottiswoode BS, Zhong X, Lorenz CH, Mayosi BM, Meintjes EM, Epstein FH. Motion-guided segmentation for cine dense MRI. *Med Image Anal* 2009; **13**: 105–15. doi: https://doi.org/10.1016/j.media.2008.06.016
38. Liu GR. Meshfree Methods: Moving Beyond the Finite Element Method.. In: ed.*2*. Boca Raton: CRC Press; 2009.
39. Wang JG, Liu GR. A point interpolation meshless method based on radial basis functions. *Int J Numer Methods Eng* 2002; **54**: 1623–48. doi: https://doi.org/10.1002/nme.489
40. Wang JG, Liu GR. On the optimal shape parameters of radial basis functions used for 2-D meshless methods. *Comput Methods Appl Mech Eng* 2002; **191**(23-24): 2611–30. doi: https://doi.org/10.1016/S0045-7825(01)00419-4
41. Sengupta PP, Tajik AJ, Chandrasekaran K, Khandheria BK. Twist mechanics of the left ventricle: principles and application. *JACC Cardiovasc Imaging* 2008; **1**: 366–76. doi: https://doi.org/10.1016/j.jcmg.2008.02.006
42. Andre F, Steen H, Matheis P, Westkott M, Breuninger K, Sander Y, et al. Age- and gender-related normal left ventricular deformation assessed by cardiovascular magnetic resonance feature tracking. *J Cardiovasc Magn Reson* 2015; **17**: 25. doi: https://doi.org/10.1186/s12968-015-0123-3
43. Cain PA, Ahl R, Hedstrom E, Ugander M, Allansdotter-Johnsson A, Friberg P, et al. Age and gender specific normal values of left ventricular mass, volume and function for gradient echo magnetic resonance imaging: a cross sectional study. *BMC Med Imaging* 2009; **9**: 2. doi: https://doi.org/10.1186/1471-2342-9-2
44. Japp AG, Gulati A, Cook SA, Cowie MR, Prasad SK. The diagnosis and evaluation of dilated cardiomyopathy. *J Am Coll Cardiol* 2016; **67**: 2996–3010. doi: https://doi.org/10.1016/j.jacc.2016.03.590
45. Sisakian H. Cardiomyopathies: evolution of pathogenesis concepts and potential for new therapies. *World J Cardiol* 2014; **6**: 478–94. doi: https://doi.org/10.4330/wjc.v6.i6.478
46. Seidman A, Hudis C, Pierri MK, Shak S, Paton V, Ashby M, et al. Cardiac dysfunction in the trastuzumab clinical trials experience. *JCO* 2002; **20**: 1215–21. doi: https://doi.org/10.1200/JCO.2002.20.5.1215
47. Tan TC, Scherrer-Crosbie M. Cardiac complications of chemotherapy: role of imaging. *Curr Treat Options Cardiovasc Med* 2014; **16**: 296. doi: https://doi.org/10.1007/s11936-014-0296-3
48. Sarfati D, Koczwara B, Jackson C. The impact of comorbidity on cancer and its treatment. *CA: A Cancer Journal for Clinicians* 2016; **66**: 337–50. doi: https://doi.org/10.3322/caac.21342